Physics Letters B 824 (2022) 136782

Contents lists available at ScienceDirect

Physics Letters B

www.elsevier.com/locate/physletb

Secondary scintillation yield in pure krypton

R.D.P. Mano, C.A.O. Henriques, F.D. Amaro, C.M.B. Monteiro *

LIBPhys-UC, Physics Department, University of Coimbra, Rua Larga, 3004-516 Coimbra, Portugal

ARTICLE INFO

Article history:
Received 11 May 2021
Received in revised form 16 October 2021
Accepted 14 November 2021
Available online 19 November 2021
Editor: B. Balantekin

Keywords:
Krypton scintillation
Dual-phase detectors
Rare event detection
Avalanche photodiodes
Double electron capture
Neutrinoless double beta decay

ABSTRACT

The absolute secondary scintillation yield is of paramount importance for modelling dual-phase or high-pressure gas detectors, to be used in contemporary and in future rare event detection experiments. In addition, the search for neutrinoless double electron capture complements the search for neutrinoless double beta decay and has been measured for ^{124}Xe in several Dark Matter and Double Beta decay detectors, operating at present. Krypton presents itself as an interesting candidate for double electron capture detection experiments. We have studied the krypton secondary scintillation yield, at room temperature, as a function of electric field in the gas scintillation gap. A large area avalanche photodiode has been used to allow the simultaneous detection of the scintillation pulses as well as the direct interaction of x-rays, the latter being used as a reference for the calculation of the number of charge carriers produced by the scintillation pulses and, thus, the determination of the number of photons impinging the photodiode. An amplification parameter of 113 photons per kV per drifting electron and a scintillation threshold of 2.7 Td (0.7 kV cm^{-1} bar^{-1} at 293 K) was obtained, in good agreement with the simulation data reported in the literature. On the other hand, the ionisation threshold in krypton was found to be around 13.5 Td (3.4 kV cm^{-1} bar^{-1}), less than what had been obtained by the most recent simulation work-package. The krypton amplification parameter is about 80% and 140% of those measured for xenon and argon, respectively.

1. Introduction

The secondary scintillation yield of gaseous xenon and argon have been studied in detail, both experimentally (e.g. see [1–7] and references therein) and through simulation tools [8–12]. At present, the main drive for those studies is the ongoing development of dual-phase [13–19] and high-pressure gaseous [20–23] optical Time Projection Chambers (TPC), which make use of the secondary scintillation, also called electroluminescence (EL), processes in the gas for the amplification of the primary ionisation signals produced by radiation interaction inside the TPC active volume. The R&D of such TPCs aims at applications to Dark Matter search [13–17] and to neutrino physics, such as neutrino oscillation [18,19], double beta decay [20–22] and double electron capture [24] detection. The physics behind these rare event detection experiments is of utmost importance in contemporary particle physics, nuclear physics and cosmology, justifying the enormous R&D efforts carried out by the scientific community.

The radioactivity of ^{85}Kr has been a drawback for the use of krypton in rare event detection experiments, being this gas the less studied one among the noble gases. To the best of our knowledge, the secondary scintillation in krypton has only been studied by simulation [8,10] and there haven't been published any experimental results, up to now, to benchmark the simulation tools. Nevertheless, there are two experiments that make use of krypton, namely the measurement of the double electron capture in ^{78}Kr [25–28] and the search for solar hadronic axions emitted in the M1 transition of ^{83}Kr nuclei [29–32]. Moreover, ^{83}Kr has also been proposed for inelastic dark matter search [33]. The enrichment of a given isotope of a noble gas is, nowadays, a matured technique, not significantly expensive, allowing for the reduction of the radioactive isotope to tolerable levels for a particular experiment.

The double-electron capture half-life is an important benchmark for nuclear structure models [34–38], providing vital experimental constraints. In addition, it presents a significant step in the search for neutrinoless double electron capture. The latter can complement the search for the neutrinoless double beta decay. Both would unveil the Majorana nature of the neutrino, access the absolute neutrino mass and contribute to understand the dominance of matter over antimatter by means of leptogenesis. On the other hand, axions and axion-like particles are potential candidates for the constituent particles of dark matter, being the main reason

* Corresponding author.
E-mail address: cristinam@uc.pt (C.M.B. Monteiro).

https://doi.org/10.1016/j.physletb.2021.136782

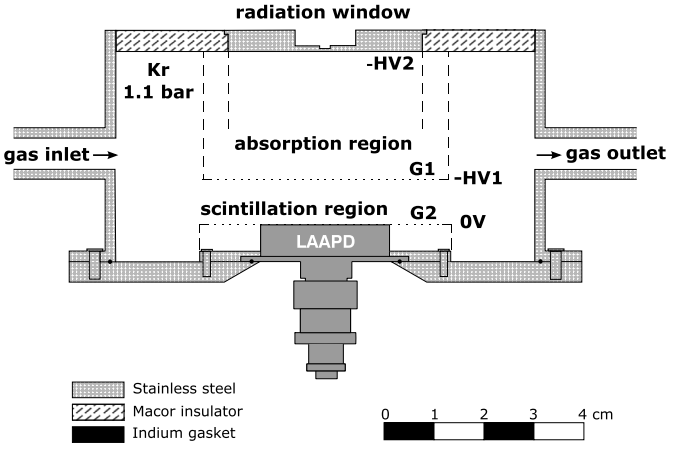

Fig. 1. Schematic of the GPSC with a large-area APD as the photosensor.

for extensive axion searches, e.g. see [39] and references therein for detailed theoretical and experimental reviews.

The referred to above rare event search experiments, having krypton as target, have been carried out with gas proportional counters using enriched krypton [25–32]. However, optical-TPCs deliver higher gains with reduced electronic noise and overly improved energy resolution when compared to proportional counters [40–43]. Furthermore, the use of a 2D-readout for the secondary scintillation signal allows the reconstruction of the topology of the ionisation event [42,43] in a more effective way than the complex analysis of the waveform associated to the ionisation events in the above-mentioned proportional counters. Therefore, the use of optical TPCs will allow larger sensitive volumes, better event discrimination and a more effective background reduction than the present proportional counters, hence having the potential for improved sensitivity and accuracy.

Having this in mind, in this work we present the experimental studies we have performed on the secondary scintillation yield of pure Kr and compare the obtained results with those attained from simulation studies [8,10]. The setup is described in Section 2, and in Section 3 we discuss the methodology that was followed in order to obtain the absolute secondary scintillation yield, while in Section 4 we present the obtained results and corresponding discussion, summarising the main conclusions in Section 5.

2. Experimental setup

In this work, we used a gas proportional scintillation counter (GPSC) [40], Fig. 1, already used in [1,3] irradiated with a 1.5-mm collimated beam of 5.9-keV x-rays emitted from a ^{55}Fe radioactive source, having a Cr filter to absorb the most part of the 6.4-keV Mn-K$_\beta$ line. The primary electron clouds resulting from the x-ray interactions in the absorption region are driven towards the scintillation region under a weak electric field, with intensity below the gas excitation threshold. The intensity of the electric field in the scintillation region is set above the gas excitation threshold, but below the ionisation threshold to prevent further electron multiplication. Upon crossing the scintillation region, the electrons are accelerated by the electric field, gaining enough energy to excite the gas media by electron impact, leading to a secondary scintillation pulse with a large number of VUV photons as a result of the gas de-excitation processes. The number of UV photons is proportional to the number of primary electrons crossing the scintillation region and, thus, to the incident x-ray energy. The detector response to x-rays has been studied in detail for Xe [46], Ar [47] and Kr [48] gas fillings.

The GPSC is depicted in Fig. 1 and has a 2.5-cm deep absorption region, a 0.9-cm deep scintillation region, and is filled with Kr at a pressure of 1.1 bar, continuously purified through St707 SAES getters [44]. G1 and G2 are stainless steel meshes, with 80-µm diameter wires and 900-µm spacing. The radiation window holder and its focusing electrode are made of stainless steel and are kept at negative voltage, while the stainless steel G2-holder and the detector body are maintained at ground potential. The voltage difference between the radiation window and G1 determines the electric field in the absorption region, while the voltage of G1 determines the electric field in the scintillation region. A Macor piece, which insulates the radiation window holder, the G1 holder and its feedthrough, is vacuum-sealed onto the stainless steel using a low-vapour pressure epoxy.

The secondary scintillation pulses are read out by a VUV-sensitive silicon large-area avalanche photodiode (LAAPD) [45], having a 16-mm diameter active area. The LAAPD is vacuum-sealed by compressing its enclosure against the detector bottom plate using an indium ring. The LAAPD signals are fed through a low-noise, 1.5 V/pC, charge pre-amplifier followed by an amplifier with 2-µs shaping time and are pulse-height analysed with a multi-channel analyser (MCA).

3. Absolute secondary scintillation yield measurement methodology

Most of the 5.9-kev x-rays interact in the absorption region producing, in the LAAPD, signals of large amplitude as a result of the secondary scintillation. Nevertheless, a small fraction of the 5.9-keV x-rays are transmitted through the gas and interact directly in the LAAPD layer producing signals with lower amplitude when compared to those resulting from the x-ray interactions in the gas. Fig. 2 depicts a typical pulse-height distribution of the signals at the LAAPD output, obtained when irradiating the detector with 5.9-keV x-rays. It includes the Kr secondary scintillation peak, more intense and in the high-amplitude region, the peak resulting from the direct interactions of the x-rays in the LAAPD, much less intense and in the low-amplitude region, and the electronic noise tail in the low-amplitude limit. Since the 5.9-keV x-rays penetrate the Kr gas volume down to the LAAPD, x-ray interactions inside the scintillation region are responsible for the tail located on the left side of the scintillation peak and extending down to the low-energy region. While the amplitude of the scintillation peak depends on both scintillation region and LAAPD biasing, the amplitude of the events resulting from direct x-ray interaction in the LAAPD depends solely on the LAAPD biasing. In addition, the latter peak is present even for a null electric field in the scintillation region and/or when the detector is under vacuum. For pulse amplitude measurements, the pulse-height distributions are fit to Gaussian functions superimposed on a linear background, from which the Gaussian centroids are determined.

The presence of the peak of direct x-ray interactions in the LAAPD is of utmost importance, as the average number of charge carriers produced in the silicon wafer by the x-ray interactions, N_{RX} is well known, as it depends only on the Si w-value and the incident x-ray energy, and is used as a reference for the secondary scintillation peak. Comparing both pulse-heights, a ratio can be found between the pulse amplitudes resulting from the secondary scintillation and from the direct x-ray absorption in the LAAPD. This ratio allows a direct quantification of the number of charge carriers produced in the LAAPD by the scintillation pulse and, thus, the number of VUV-photons impinging the LAAPD, given its quantum efficiency. The simultaneous detection of the light pulses and the x-rays in the photosensor under the same conditions in the same setup allows a straightforward measurement of the number of photons impinging the photosensor. This method has been used for measuring Xe and Ar absolute secondary scintillation yield in

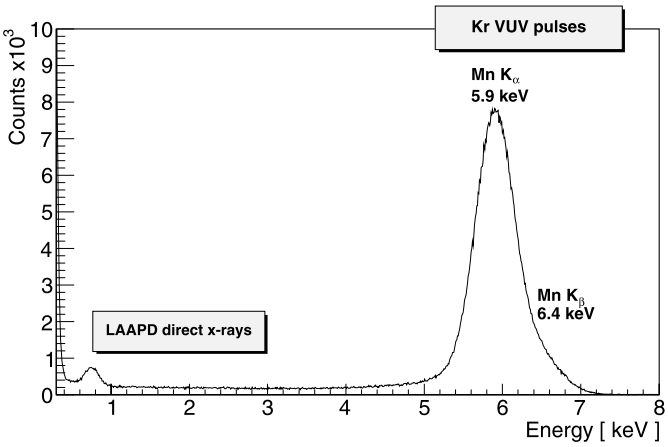

Fig. 2. Typical pulse-height distribution obtained for 5.9-keV x-rays from a ^{55}Fe radioactive source and electric field intensities of 0.34- and 3.4 kV cm^{-1} bar^{-1} in the absorption and scintillation region, respectively. The LAAPD bias was 1840 V, corresponding to a gain of $\sim$ 150.

uniform electric fields [1,3] and in electron avalanches of GEMs, THGEMs and Micromegas micropatterned structures [49,50].

The number of charge carriers produced in the LAAPD by the secondary scintillation pulse is:

$$N_{VUV} = \left(\frac{A_{EL}}{A_{RX}}\right) N_{RX} \tag{1}$$

being A_{RX} and A_{EL} the amplitude of the peaks resulting from the direct x-ray interactions in the LAAPD and from the scintillation produced by the x-ray interactions in the gas, respectively, read in the MCA. The non-linear response of the LAAPD to 5.9-keV x-rays, e.g. see Fig. 20 of [51], was considered and the ratio A_{EL}/A_{RX} was corrected for this effect. A factor of 0.94 was used in this correction, for the LAAPD biasing voltage of 1840 V used throughout this work, which corresponds to a LAAPD gain of about 150. Knowing the quantum efficiency, QE, of the LAAPD, the optical transparency of G2, T, and the fraction of the average solid angle, $\Omega_f = \Omega/4\pi$ subtended by the active area of the photosensor relative to the primary electron path, the total number of photons produced in the secondary scintillation pulse is obtained by:

$$N_{total,VUV} = \left(\frac{A_{EL}}{A_{RX}}\right) \frac{N_{RX}}{QE \times T \times \Omega_f} \tag{2}$$

The secondary scintillation yield is defined as the number of photons in the pulse-height distribution produced per drifting primary electron and per unit path length,

$$Y = \left(\frac{A_{EL}}{A_{RX}}\right) \frac{N_{RX}}{QE \times T \times \Omega_f \times N_e \times d} \tag{3}$$

where N_e is the number of primary electrons produced in Kr by a 5.9-kev x-ray interaction and d is the scintillation region depth.

Since the w-value in silicon is 3.62 eV, e.g. [52] and references therein, the average number of free electrons produced in the LAAPD by the full absorption of the 5.9-keV x-rays is $N_{RX} = 1.63 \times 10^3$ electrons. The w-value for Kr is 24.2 eV [53], hence being $N_e = 244$ electrons. The optical transmission of G2 mesh is $T = 83\%$ and the fraction of the average solid angle has been computed by Monte Carlo simulation [54] to be $\Omega_f = 0.215$. Since the x-ray beam is highly collimated and the range of $\sim$4-keV photoelectrons in the 1.1-bar Kr is less than 1 mm, the fluctuations in the average solid angle subtended by the secondary scintillation are less than 1%, contributing much less to the amplitude fluctuations than the fluctuations inherent to the primary electron cloud formation.

At atmospheric pressures, the secondary scintillation of Kr consists of a narrow line peaking at 148 nm with 5 nm FWHM [55], called second continuum. The emissions in the visible and in the IR regions are below a few percent when compared to those in the VUV range [55,56], thus its contribution has been considered negligible. The processes leading to emission in the second continuum can be schematized as

$$e^- + Kr \rightarrow e^- + Kr^*$$

$$Kr^* + 2Kr \rightarrow Kr_2^* + Kr,$$

$$Kr_2^* \rightarrow 2Kr + h\nu$$

The electron impact with Kr atoms induces excited atoms, which through three-body collisions create excited excimers, Kr_2^*, that decay emitting one VUV photon, $h\nu$. It corresponds to transitions of the singlet and triplet bound molecular states, from vibrationally relaxed levels, to the repulsive ground state.

A LAAPD QE of 0.90 was measured for Kr secondary scintillation [57]. According to the manufacturer, the LAAPD fabrication technology is well established, and quite good reproducibility is obtained and it is expected that the behaviour observed for individual LAAPDs is representative for any of these devices. In fact [58], have measured the relative QE of $\sim$600 LAAPDs and obtained an approximately Gaussian distribution with a FWHM of $\sim$0.1. Therefore, we have considered an uncertainty of ± 0.08 ($\sim 2\sigma$) for the LAAPD QE, being this the major source of uncertainty in our measurements.

4. Experimental results and discussion

In Fig. 3 we depict the reduced secondary scintillation yield, Y/N, i.e. the secondary scintillation yield divided by the number density of the gas, as a function of reduced electric field, E/N, in the scintillation region. The data was taken using a constant electric field of 0.36 kV/cm in the absorption region, while varying the electric field in the scintillation region. Three independent runs have been performed with several days of interval and with a room temperature between 25°C and 26°C, showing a good reproducibility of the experimental results. A straight line fit provides a good description of the dependence of the reduced secondary scintillation yield with reduced electric field in the 2.5–14 Td range, a behaviour similar to that of Ar and Xe and mixtures of Xe with He or with molecular additives [1–12]. For each run, Fig. 3 also depicts a straight line fit superimposed to the experimental data, excluding the two data points taken at the highest reduced electric field values, where secondary ionisation is already non-negligible. Simulation results from [8,10] are also depicted for comparison. To the best of our knowledge, there are no other experimental or simulation results in the literature.

The reduced scintillation yield can be approximately represented as

$$\begin{aligned} &Y/N\ (10^{-17}\ \text{photons electron}^{-1}\,\text{cm}^2\,\text{atom}^{-1}) \\ &\quad = 0.113\ E/N - 0.30, \end{aligned} \tag{4}$$

where E/N is given in Td (10^{-17} V cm^2 atom^{-1}). This equation can be presented as a function of pressure, at the temperature used to convert the gas density into pressure. At room temperature Eq. (4) can be expressed as

$$Y/p\ (\text{photons electron}^{-1}\,\text{cm}^{-1}\,\text{bar}^{-1}) = 113\ E/p - 74 \tag{5}$$

The slope of the straight line fit presents the scintillation amplification parameter, i.e., the number of photons produced per drifting electron and per volt, and is in good agreement with what has

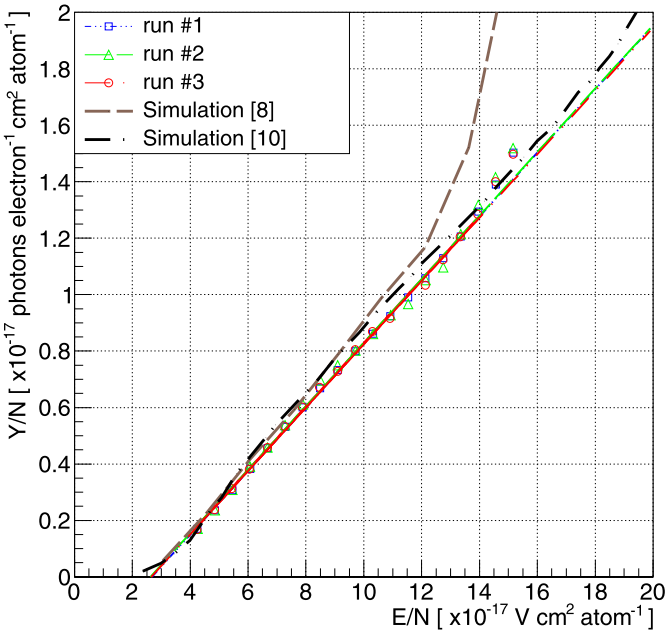

Fig. 3. Krypton reduced secondary scintillation yield as a function of reduced electric field for three different runs (this work) and the respective straight line fit to the data below 14 Td, as well as for data obtained from Monte Carlo simulation [8,10].

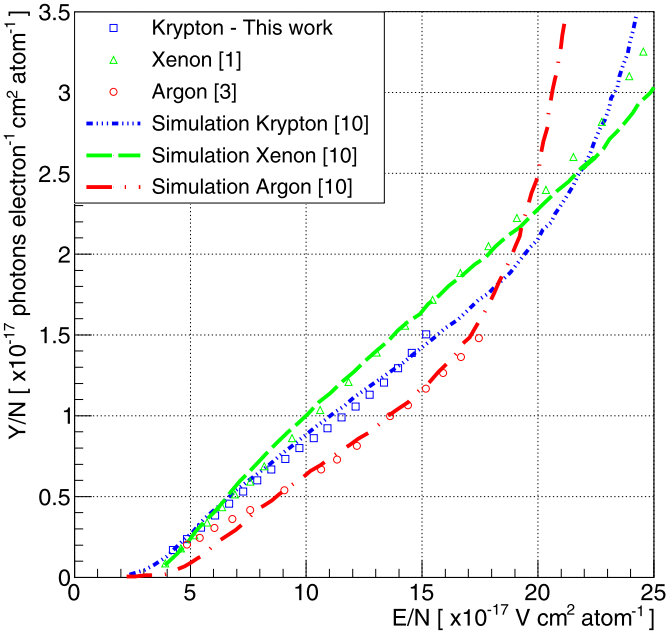

Fig. 4. Reduced secondary scintillation yield in Xe, Kr and Ar as a function of reduced electric field. Data points correspond to experimental data from [1], this work and [3], respectively, while the curves correspond to simulation data [10].

been obtained by Monte Carlo simulation for room temperature [8,10]. In addition, the excitation threshold for Kr, defined as the extrapolation of the straight line fit to zero scintillation, 2.7 Td (0.7 $\mathrm{kV\,cm^{-1}\,bar^{-1}}$ at 293 K), is also in good agreement with the values presented in the literature [8,10,59]. On the other hand, at a reduced electric field of 14 Td (3.5 $\mathrm{kV\,cm^{-1}\,bar^{-1}}$) the experimental data depart from the straight line fit, denoting already the presence of a non-negligible amount of charge multiplication in the scintillation region. Therefore, from the experimental data we can conclude that the Kr ionisation threshold should be around 13.5 Td (3.4 $\mathrm{kV\,cm^{-1}\,bar^{-1}}$). This value is higher than that obtained by MC simulation of [8] and is lower than foreseen by the most recent simulation toolkit [10], demonstrating the importance of the data obtained in this work for the development of future optical-TPCs based on Kr filling.

For comparison, Fig. 4 depicts the experimental results obtained with the present method for the secondary scintillation yield in Xe [1], Kr (this work) and Ar [3] along with the respective simulation results obtained by the most recent simulation work package for secondary scintillation production in noble gases [10]. The scintillation amplification parameter in Kr and Ar is about 80% and 60%, respectively, of that for Xe.

5. Conclusions

We have performed experimental studies on the absolute secondary scintillation yield of pure Kr at room temperature and compared it with the values obtained by Monte Carlo simulation. For the experimental measurements we used a gas proportional scintillation counter (GPSC), having a VUV-sensitive large area avalanche photodiode (LAAPD) for the scintillation readout. We used 5.9-keV x-rays to induce the secondary scintillation in the GPSC active volume or to interact directly in the LAAPD. The simultaneous detection of the secondary scintillation pulses and the x-rays in interacting directly in the photosensor under the same conditions and in the same setup, allows to use the number of charge carriers produced by the x-rays interacting directly in the LAAPD as a reference to determine the number of charge carriers produced by the secondary scintillation in the LAAPD, allowing a straightforward measurement of the number of photons impinging the photosensor. The absolute secondary scintillation yield dependence with reduced electric field is well described by a straight line fit, having an amplification parameter of 113 photons per kV, per electron, and the scintillation threshold of Kr was measured to be 2.7 Td (0.7 $\mathrm{kV\,cm^{-1}\,bar^{-1}}$ at 293 K), in good agreement with the simulation data in the literature. Above 14 Td (3.5 $\mathrm{kV\,cm^{-1}\,bar^{-1}}$) the secondary scintillation yield departs from the straight line fit, showing a faster increase due to the additional scintillation produced by extra secondary electrons resulting from the charge multiplication onset. The Kr amplification parameter is around 80% and 140% of that measured for Xe and Ar, respectively.

Declaration of competing interest

The authors declare that they have no known competing financial interests or personal relationships that could have appeared to influence the work reported in this paper.

Acknowledgements

This work is funded by portuguese national funds, through FCT — Fundação para a Ciência e Tecnologia, I.P. in the scope of the project UIDP/04559/2020 (LIBPhys).

References

[1] C.M.B. Monteiro, et al., Secondary scintillation yield in pure xenon, J. Instrum. 2 (2007) P05001.
[2] E.D.C. Freitas, et al., Secondary scintillation yield in high-pressure xenon gas for neutrinoless double beta decay ($0\nu\beta\beta$) search, Phys. Lett. B 684 (2010) 205.
[3] C.M.B. Monteiro, et al., Secondary scintillation yield in pure argon, Phys. Lett. B 668 (2008) 167.
[4] A. Buzulutskov, et al., Revealing neutral bremsstrahlung in two-phase argon electroluminescence, Astropart. Phys. 103 (2018) 29.
[5] C.A.O. Henriques, et al., NEXT Collaboration, Secondary scintillation yield of xenon with sub-percent levels of CO_2 additive for rare-event detection, Phys. Lett. B 773 (2017) 663.
[6] C.A.O. Henriques, et al., NEXT Collaboration, Electroluminescence TPCs at the thermal diffusion limit, J. High Energy Phys. 1 (2019) 027.

[7] A.F.M. Fernandes, et al., NEXT Collaboration, Electroluminescence yield in low-diffusion Xe-He gas mixtures for rare-event detection, J. High Energy Phys. 34 (2020) 034.

[8] T.H.V.T. Dias, et al., A unidimensional Monte-Carlo simulation of electron drift velocities and electroluminescence in argon, krypton and xenon, J. Phys. D, Appl. Phys. 19 (1986) 527.

[9] F.P. Santos, et al., 3-dimensional Monte-Carlo calculation of the VUV electroluminescence and other electron-transport parameters in xenon, J. Phys. D, Appl. Phys. 27 (1994) 42.

[10] C.A.B. Oliveira, et al., A simulation toolkit for electroluminescence assessment in rare event experiments, Phys. Lett. B 703 (2011) 217.

[11] C.A.B. Oliveira, et al., Energy resolution studies for NEXT, J. Instrum. 6 (2011) P05007.

[12] C.D.R. Azevedo, et al., NEXT Collaboration, Microscopic simulation of xenon-based optical TPCs in the presence of molecular additives, Nucl. Instrum. Methods Phys. Res., Sect. A 877 (2018) 157.

[13] K. Pushkin, LZ Collaboration, Direct search for WIMP dark matter particles with the LUX-ZEPLIN (LZ) detector, Nucl. Instrum. Methods Phys. Res., Sect. A 936 (2019) 162.

[14] X. Cui, et al., PandaX-II collaboration, Dark matter results from 54-ton-day exposure of PandaX-II experiment, Phys. Rev. Lett. 119 (2017) 181302.

[15] E. Aprile, et al., XENON Collaboration, The XENON1T dark matter experiment, Eur. Phys. J. C 77 (2017) 881.

[16] J. Aalbers, et al., DARWIN: towards the ultimate dark matter detector, J. Cosmol. Astropart. Phys. 11 (2016) 017.

[17] P. Agnes, et al., DarkSide Collaboration, DarkSide-50 532-day dark matter search with low-radioactivity argon, Phys. Rev. D 98 (2018) 102006.

[18] B. Aimard, et al., A 4 tonne demonstrator for large-scale dual-phase liquid argon time projection chambers, J. Instrum. 13 (2018) P11003.

[19] T. Lux, Charge and light production in the charge readout system of a dual phase LAr TPC, J. Instrum. 14 (2019) P03006.

[20] J. Martin-Albo, et al., NEXT Collaboration, Sensitivity of NEXT-100 to neutrinoless double beta decay, J. High Energy Phys. 5 (2016) 159.

[21] K. Nakamura, et al., AXEL-a high pressure xenon gas TPC for neutrinoless double beta decay search, Nucl. Instrum. Methods Phys. Res., Sect. A 845 (2017) 394.

[22] A. Fieguth, Search for double beta-decays of Xe-124 with XENON100 & XENON1T, J. Phys. Conf. Ser. 888 (2017) 012251.

[23] D. Gonzalez-Diaz, et al., Gaseous and dual-phase time projection chambers for imaging rare processes, Nucl. Instrum. Methods Phys. Res., Sect. A 878 (2018) 200.

[24] E. Aprile, et al., XENON Collaboration, Observation of two-neutrino double electron capture in Xe-124 with XENON1T, Nature 568 (2019) 532.

[25] Yu.M. Gavrilyuk, et al., Indications of $2\nu 2K$ capture in ^{78}Kr, Phys. Rev. C 87 (2013) 035501.

[26] S. Bustabad, et al., Examination of the possible enhancement of neutrinoless double-electron capture in Kr-78, Phys. Rev. C 88 (2013) 035502.

[27] S.S. Ratkevich, et al., Comparative study of the double-K-shell-vacancy production in single- and double-electron-capture decay, Phys. Rev. C 96 (2017) 065502.

[28] Yu.M. Gavrilyuk, et al., Results of in-depth analysis of data obtained in the experimental search for $2K(2\nu)$-capture in ^{78}Kr, Phys. Part. Nucl. 49 (2018) 540.

[29] Yu.M. Gavrilyuk, et al., New experiment on search for the resonance absorption of solar axion emitted in the M1 transition of ^{83}Kr nuclei, JETP Lett. 101 (2015) 664.

[30] Yu.M. Gavrilyuk, et al., Search for resonant absorption of solar axions emitted in M1-transitions in ^{83}Kr nuclei: second stage of the experiment, Phys. Part. Nucl. 49 (2018) 94.

[31] Z.A. Akhmatov, et al., Results of searching for solar hadronic axions emitted in the M1 transition in ^{83}Kr nuclei, Phys. Part. Nucl. 49 (2018) 599.

[32] Yu.M. Gavrilyuk, et al., New constraints on the axion–photon coupling constant for solar axions, JETP Lett. 107 (2018) 589.

[33] J.D. Vergados, et al., Theoretical direct WIMP detection rates for transitions to the first excited state in Kr-83, Phys. Rev. D 92 (2015) 015015.

[34] M. Hirsch, et al., Nuclear-structure calculation of Beta+Beta+, Beta+ EC and EC EC decay matrix-elements, Z. Phys. A, Hadrons Nucl. 347 (1994) 151.

[35] M. Aunola, J. Suhonen, Systematic study of beta and double beta decay to excited final states, Nucl. Phys. A 602 (1996) 133.

[36] J. Suhonen, Analysis of double-beta transitions in Kr-78, Phys. Rev. C 87 (2013) 034318.

[37] J. Suhonen, On the neutrinoless double beta(+)/EC decays, AIP Conf. Proc. 1572 (2013) 102;
L. Maalampi, J. Suhonen, Neutrinoless double beta(+)/EC decays, Adv. High Energy Phys. (2013) 505874.

[38] E.A.C. Perez, et al., Two-neutrino double electron capture on 124Xe based on an effective theory and the nuclear shell model, Phys. Lett. B 797 (2019), UNSP 134885.

[39] M. Tanabashi, et al., Particle Data Group, Review of Particle Physics, Phys. Rev. D 98 (2018) 030001.

[40] J.M.F. dos Santos, et al., Development of portable gas proportional scintillation counters for x-ray spectrometry, X-Ray Spectrom. 30 (2001) 373.

[41] C.M.B. Monteiro, et al., Secondary scintillation yield from gaseous micropattern electron multipliers in direct dark matter detection, Phys. Lett. B 677 (2009) 133.

[42] F. Monrabal, et al., NEXT collaboration, The NEXT White (NEW) detector, J. Instrum. 13 (2018) P12010.

[43] F.M. Brunbauer, et al., Live event reconstruction in an optically read out GEM-based TPC, Nucl. Instrum. Methods Phys. Res., Sect. A 886 (2018) 24.

[44] SAES Advanced Technologies SpA, Nucleo Industriale, CP 9367 051, Avezzano (AQ), Italy.

[45] Deep-UV enhanced series, Advanced Photonix, Inc., 1240 Avenida Acaso, Camarillo, CA 93012, USA.

[46] J.A.M. Lopes, et al., A xenon gas proportional scintillation counter with a UV-sensitive large-area avalanche photodiode, IEEE Trans. Nucl. Sci. 48 (2001) 312.

[47] C.M.B. Monteiro, et al., An argon gas proportional scintillation counter with UV avalanche photodiode scintillation readout, IEEE Trans. Nucl. Sci. 48 (2001) 1081.

[48] C.M.B. Monteiro, et al., A gas proportional scintillation counter with krypton filling, J. Instrum. 11 (2016) C12079.

[49] C.M.B. Monteiro, et al., Secondary scintillation yield from GEM and THGEM gaseous electron multipliers for direct dark matter search, Phys. Lett. B 714 (2012) 18.

[50] C. Balan, et al., MicrOMEGAs operation in high pressure xenon: charge and scintillation readout, J. Instrum. 6 (2011) P02006.

[51] L.M.P. Fernandes, et al., Characterization of large area avalanche photodiodes in X-ray and VUV-light detection, J. Instrum. 2 (2007) P08005.

[52] F. Gao, et al., Monte Carlo method for simulating gamma-ray interaction with materials: a case study on Si, Nucl. Instrum. Methods Phys. Res., Sect. A 579 (2007) 292.

[53] L.K. Bronic, W values and Fano factors for electrons in rare gases and rare gas mixtures, Hoshasen: Ionizing Radiation 24 (1998) 101, https://studylib.net/doc/5876359/%E2%80%9Av-values-and-fano-factors-for-electrons-in-rare.

[54] J.M.F. dos Santos, et al., The dependence of the energy resolution of gas proportional scintillation counters on the scintillation region to photomultiplier distance, IEEE Trans. Nucl. Sci. 39 (1992) 541.

[55] M. Suzuki, S. Kubota, Mechanism of proportional scintillation in argon, krypton and xenon, Nucl. Instrum. Methods 164 (1979) 197.

[56] C.A.B. Oliveira, et al., Simulation of gaseous Ar and Xe electroluminescence in the near infrared range, Nucl. Instrum. Methods Phys. Res., Sect. A 722 (2013) 1.

[57] R. Chandrasekharan, et al., Detection of noble gas scintillation light with large area avalanche photodiodes (LAAPDs), Nucl. Instrum. Methods Phys. Res., Sect. A 546 (2005) 426.

[58] R. Neilson, et al., Characterization of large area APDs for the EXO-200 detector, Nucl. Instrum. Methods Phys. Res., Sect. A 608 (2009) 68.

[59] M.A. Feio, et al., Thresholds for secondary light-emission by noble-gases, Jpn. J. Appl. Phys. 21 (1982) 1184, and references therein.